

https://doi.org/10.1070/QEL16301

Generation of attosecond electron packets in the interaction of ultraintense Laguerre–Gaussian laser beams with plasma

C. Baumann, A.M. Pukhov

Abstract. **The interaction of a thin plasma foil with two counterpropagating circularly polarised Laguerre–Gaussian laser beams of ultra-high intensity is studied using pwarticle-in-cell simulations in a fully three-dimensional geometry. It is found that within the course of the interaction, bunched electron packets are generated from the plasma target. Each packet has a duration of about 830 attoseconds, and adjacent bunches are spatially separated by one laser wavelength. The emitted electron packets move at ultrarelativistic velocities along the axis of laser propagation.**

Keywords: *ultra-intense laser pulses, Laguerre–Gaussian modes, gamma-ray generation, particle-in-cell simulations.*

1. Introduction

Since the development of the fundamental concept of lasers and their first realisation, the continuous progress in laser technology has improved the understanding of many physical systems and has opened the possibility of studying new physics. State-of-the-art lasers are already able to achieve peak intensities of the order of $\sim 10^{22}$ W cm^{-2} [1], and current projects [2, 3] aim at reaching at least intensities of 10^{23} W cm^{-2}. Thus, it will be possible to investigate the behaviour of matter in ultraintense fields. In this intensity regime, there are several processes which may influence the laser–plasma interaction like, for instance, radiation damping due to nonlinear Compton scattering and electron–positron production [4]. Radiation damping influences especially the electron dynamics. Instead of being directly expelled by the ponderomotive force, electrons can stay in ultraintense electromagnetic fields for a time that is significantly longer than in the case if one ignores radiation damping [5–8]. In most previous works, simple Gaussian laser modes have been typically used to study the laser–plasma interaction in ultraintense fields. Even if other laser modes such as Laguerre–Gaussian beams are intensively considered (see [9] and references therein), these modes are used rather rarely in the quantum-dominated regime [10]. This paper presents studies on the interaction of a thin plasma foil with two counterpropagating circularly polarised Laguerre–Gaussian laser pulses, thereby generating a train of ultrashort electron packets. The generation of such electron bunches is being intensively studied (see for instance [11, 12]), since it allows for new insights in physical processes that takes place on ultrashort timescales.

The paper is organised as follows. In section II, the reader can find a short description of the simulation setup, especially the used plasma and laser parameters are introduced. In the following section, the results of the particle-in-cell simulations are shown and the observed generation of ultrashort electron packets is discussed. Finally, section IV concludes the main aspects of this work.

C. Baumann, A.M. Pukhov Institut für Theoretische Physik I, Heinrich-Heine-Universität Düsseldorf, 40225 Düsseldorf, Germany;
e-mail: christoph.baumann@tp1.uni-duesseldorf.de, pukhov@tp1.uni-duesseldorf.de

Received 6 February 2017
Kvantovaya Elektronika **47** (3) 194–198 (2017)
Submitted in English

2. Simulation setup

The particle-in-cell (PIC) simulations are performed in a three-dimensional (3D) geometry using the Virtual Laser Plasma Lab (VLPL) code [13]. The simulation box has an extension of $20\lambda_0$, $25\lambda_0$ and $25\lambda_0$ in x, y and z directions ($\lambda_0 =$ 1 μm is the laser wavelength), with a spatial grid step of $0.05\lambda_0 \times 0.075\lambda_0 \times 0.075\lambda_0$, respectively. The time step has been chosen such that the Courant condition is satisfied. The plasma target is a one micron thick foil with an ion mass-to-charge ratio of two times that of protons. The plasma is represented by ten macroparticles per species and cell.

Initially the foil is located in the centre of the simulation box. The initial electron density is $50n_{\rm cr}$, where $n_{\rm cr} \approx 1.12 \times 10^{21}$ cm^{-3} is the critical density for the considered wavelength. In transverse direction, periodic boundary conditions are used for each particle species. This is different to the longitudinal direction where absorbing boundary conditions have been established.

There are two laser beams that counterpropagate along the x axis and that impinge at normal incidence on the target. These laser pulses were modelled as circularly polarised (CP) Laguerre–Gaussian modes. Both carrier waves have opposite helicities and a zero phase difference between the y-component of their electric fields*. According to [14], the electric field profile of a Laguerre–Gaussian mode can be expressed as

$$E_p^m(r,\varphi,x) = C_p^{|m|}A(x)\left(\frac{\sqrt{2}\,r}{w(x)}\right)^{|m|}L_p^{|m|}\left(\frac{2r^2}{w^2(x)}\right) \times \exp(\mathrm{i}m\varphi)\exp\left[-\frac{\mathrm{i}\pi r^2}{\lambda_0 q(x)}\right], \quad (1)$$

* In particular, the right-moving laser beam has right-handed polarisation, whereas the left-moving laser beam has left-landed polarisation. The polarisation state is defined from the point of view of the corresponding radiation source. The carrier wave of the E_y component is given by $E_y = -\sin[2\pi(t \pm x)]$, where the upper (lower) sign corresponds to the left- (right-) moving pulse.

where p, m are integers representing the mode; $C_p^{|m|}$ is a normalisation constant; L_p^m are the generalised Laguerre polynomials; and $A(x)$, $q(x)$ and $\omega(x)$ are characteristic functions that are defined in [14]. In the present work, $p = 0$ and $m = 1$ have been chosen. This mode is also referred to as doughnut mode. Each of the laser pulses has a peak intensity of 6.86×10^{23} W cm^{-2}. This intensity corresponds to a dimensionless field amplitude of $a_0 = 500$. The pulse duration is chosen to be roughly 20 fs at full width at half maximum (FWHM) and the transverse spread is equal to approximately 4 μm (FWHM). Absorbing conditions have been used for the electromagnetic field to suppress nonphysical reflections at the boundaries.

The PIC code VLPL has a special module, which can describe quantum electrodynamical (QED) events which become relevant in ultraintense fields. The dominant processes are hard photon emission by nonlinear Compton scattering and electron–positron generation by the multiphoton Breit–Wheeler process. However, note that the pair production is not considered in the present work, since simulations with Gaussian pulses in a 2D geometry indicate that pairs do not change the laser–plasma interaction significantly at the intensity of interest [8]. Further information about the implementation of QED events in PIC codes and especially in VLPL can be found in [15–17] and [8], respectively.

Throughout the paper, time is measured with respect to the point at which the peak value of each pulse reaches the centre of the simulation box.

3. Results

Both laser beams are impinging at normal incidence onto the plasma target. At the beginning, one can observe a symmetrical compression of the plasma target in the high-intensity region of the Laguerre–Gaussian pulses (see Fig. 1a). This can be attributed to the ponderomotive force which accelerates electrons in the direction of motion of the pushing laser.

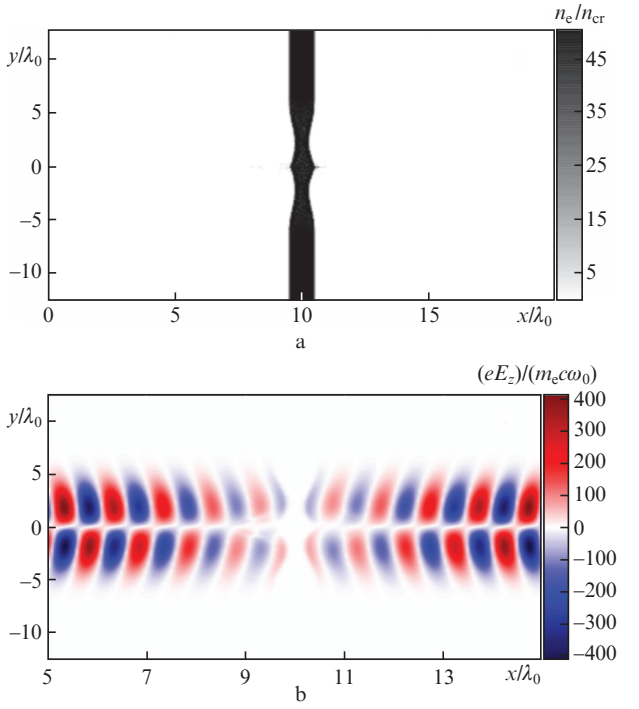

Figure 1. Cross section in the xy plane with $z = 0\lambda_0$ of (a) the electron density and (b) of the z-component of the magnetic field at a time moment $t \approx -5T_0$ (T_0 is the period of the laser field).

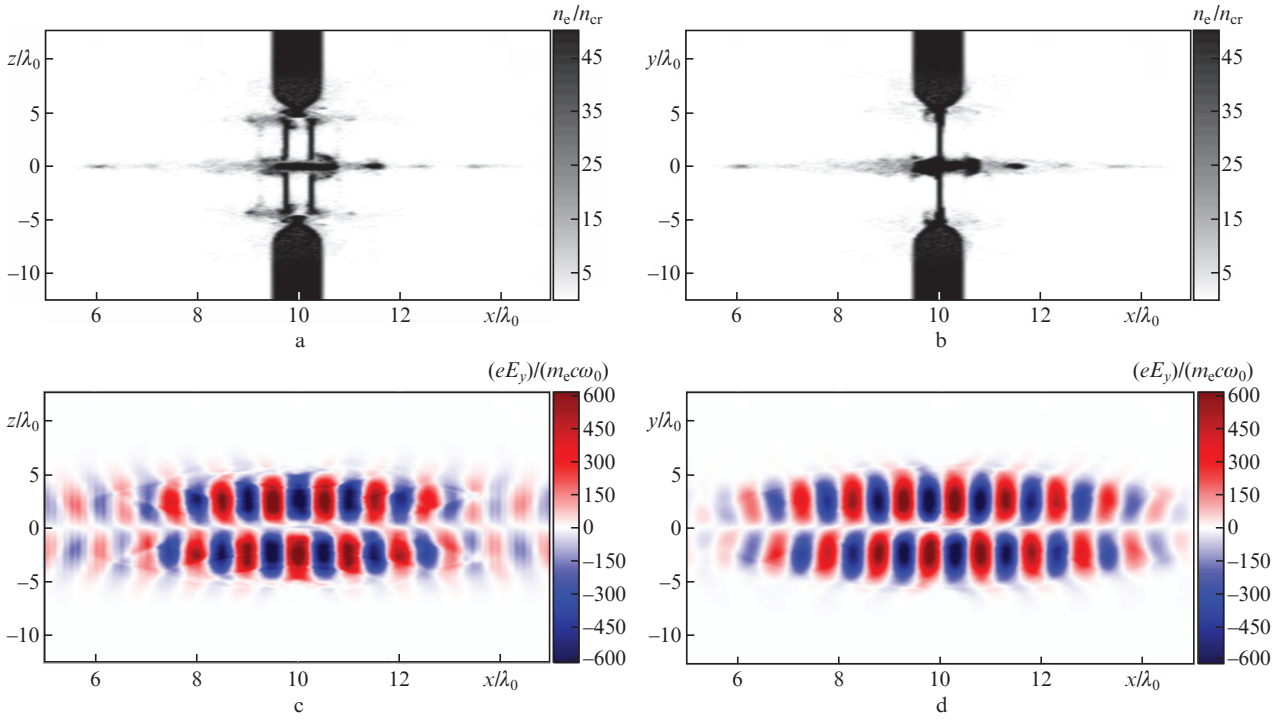

Figure 2. Cross sections of the electron density in (a) the xz plane with $y = 0\lambda_0$ and in (b) the xy plane with $z = 0\lambda_0$, as well as cross sections of the y-component of the electric field in (c) the xz and (d) xy plane, respectively. All snapshots are taken at an interaction time of $t \approx 0T_0$.

Since the target itself is over-dense, the incoming radiation cannot penetrate the plasma and gets reflected at the targets' surface (see Fig. 1b). However, with increasing interaction time electrons are accelerated to large Lorentz factors ($\gamma \sim a_0$) which leads to an effective reduction of the plasma frequency, $\omega_p^{\text{eff}} \approx \omega_p/\sqrt{a_0}$. As a result, the plasma becomes transparent for the incident laser light. It develops an electromagnetic field structure that can trap electrons in nodes of the electric field due to the increasing influence of nonlinear Compton scattering on the laser–plasma interaction (see [8]). This can be seen for instance in Figs 2a and 2c, where cross sections of the electron density and of the electric y-component are shown in the xz plane. Here, electrons are mainly focused to the electrical node positions at $x = 9.75\lambda_0$ and $10.25\lambda_0$. On the other hand, Figs 2b and 2d visualise the same cross sections in the xy plane. One can see that electrons are only focused at $x = 10\lambda_0$ such that the electronic structure is not rotationally symmetric with respect to the axis of laser propagation. This is caused by the Laguerre–Gaussian modes which have, according to Eqn (1), an explicit dependence on the azimuthal angle for the nonvanishing parameter m. It follows that the full 3D trapping geometry is more complex than one would expect for simple Gaussian pulses. Apart from that, Fig. 2 also displays that the trapping structure is not continuous in the y and z directions and that electrons are also present in the complete zero-intensity region of the Laguerre–Gaussian mode.

Figure 3 shows cross sections of the electron density when the intensity maximum of the laser beams hits the target after roughly four laser periods. Figure 3a also demonstrates the cross section of the electron density in the xz plane. One can see that radiation damping starts to get less powerful to maintain radiative trapping in the electrical nodes at $x = 9.75\lambda_0$ and $10.25\lambda_0$, leading to a decrease in the density of trapped electrons.

There is another important aspect that needs to be addressed. The snapshot in Fig. 3a clearly indicates that electron bunches have been generated during the interaction. These packets now move in positive as well as in negative x directions. However, their particular properties depend on whether these packets move from left to right or vice versa. The reason for this is connected to the $\exp(im\varphi)$ term in Eqn (1) and will be shortly outlined at the end of this section. Considering again electrons in Fig. 3a that move towards the right boundary of the simulation box, one can identify one bunched beam that consists of five electron packets. These different electron packets are here separated by one laser wavelength in the x direction (see also Fig. 3c). In contrast, the second beam splits up in two 'jets' which move parallel to the negative x axis at a lateral distance of approximately 2.5 μm. The simulation data further suggest that these jets are moving on two helical trajectories around the x axis.

Figure 3b contains information about the transverse shape of an exemplary electron packet, recorded at a longitudinal position of $x = 12.55\lambda_0$. One can directly notice the large electron concentration around $r \approx 0\lambda_0$, where $r^2 = y^2 + z^2$ describes the radial distance from the centre. The electron density is here roughly 100 n_{cr} (see Fig. 3c). This high-density region is surrounded by an annulus, consisting of an inner circle with radius $R_{in} \approx 1.5\lambda_0$ and an outer circle with radius $R_{ex} \approx 5\lambda_0$, in which no electrons are present. The dimensions of the annulus coincide with those of the trapping structure in the y and z directions. In this way, the beam quality is significantly enhanced. Figure 3c finally shows the electron density along the x axis for fixed $y = z = 0\lambda_0$. It can be used to get detailed information about the bunch density and the bunch width in the propagation direction. One can clearly see that the generated bunches are over-dense and that adjacent packets are indeed separated by the wavelength. Similarly, it is found that

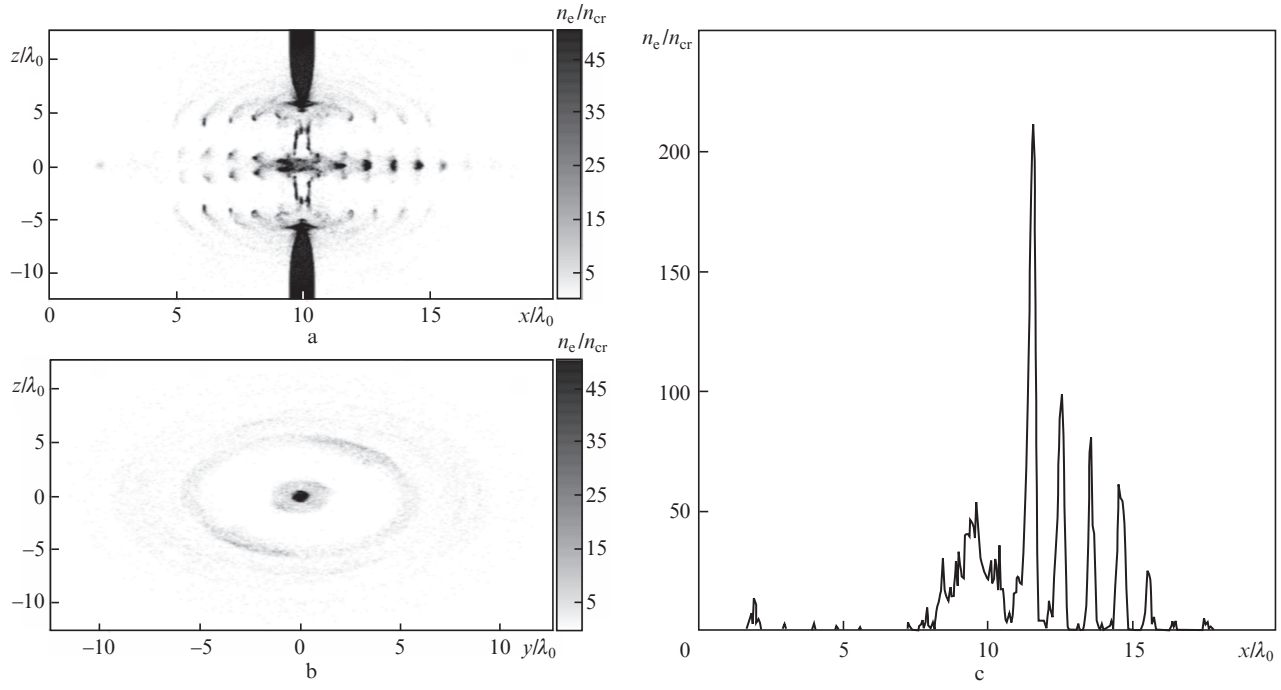

Figure 3. Cross sections of the electron density in (a) the xz plane with $y = 0\lambda_0$ and in (b) the yz plane with $x = 12.55\lambda_0$, as well as (c) electron density along the x axis for fixed y- and z-components ($y = z = 0\lambda_0$) at the moment in time $t \approx 4T_0$.

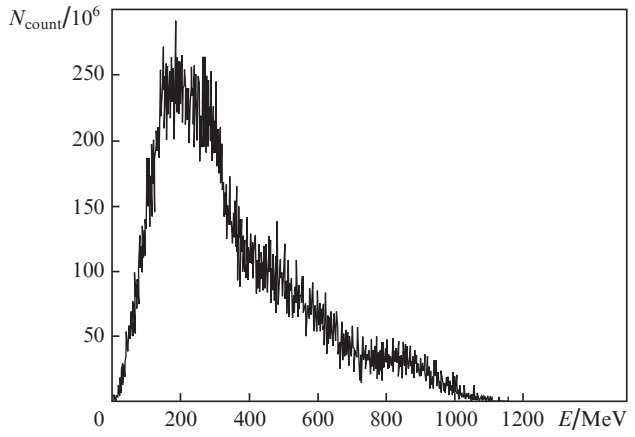

Figure 4. Energy distribution of bunch electrons at time $t = 4T_0$. The bunch contains all electrons that are in the volume $x > 11\lambda_0$ within a radius of $0.75\lambda_0$ around the x axis.

each individual electron packet has a width of almost $0.25\lambda_0$ (FWHM) in the x direction, which corresponds to a duration of 830 as in the time domain.

Figure 4 shows the energy distribution of bunch electrons that move in the positive x direction at an interaction time of $t \approx 4T_0$. The spectrum has a peak at about 200 MeV, corresponding to a Lorentz factor of $\gamma = 400$. It is in reasonable agreement with the dimensionless field amplitude of $a_0 = 500$. Thus, the described configuration generates a train of electron packets with energies of the order of a_0.

As a last point, let us briefly discuss the difference between left- and right-moving electrons. It has been already mentioned that the asymmetry is related to the $\exp(im\varphi)$ factor in Eqn (1). In the presented results, $m = 1$ has been chosen for both laser beams. Following previous works [10, 18], each laser photon thus carries an orbital angular momentum. According to the convention used in this paper, an orbital angular momentum per laser photon is assigned to the left-moving ($+\hbar$) and to the right-moving ($-\hbar$) pulse. On the other hand, the spin angular momentum is related to the combination of the helicity and the propagation direction of the laser photon. The particle has a positive helicity, if its spin and direction of motion coincide, and a negative helicity in the opposite case. As a consequence (see the footnote on page 194), each laser photon hence carries a spin angular momentum of $\hbar$, regardless of whether the laser photon is moving left or right. The sum of orbital and spin angular momenta therefore differs for both lasers and electrons effectively interact with different pulses. One can see from Fig. 3a that a total angular momentum equal to $0\hbar$ generates only one bunch, while a total angular momentum equal to $+2\hbar$ leads to an effective separation in two beams that move along helices around the x axis. To change this disparity, $m = -1$ has been used for the left-moving pulse. The results are shown in Fig. 5, with a cross section (xz plane) of the electron density at $t \approx 2T_0$. In this setup of colliding pulses, the disparity is removed such that one can observe only one centred beam of electron packets on each side of the plasma target.

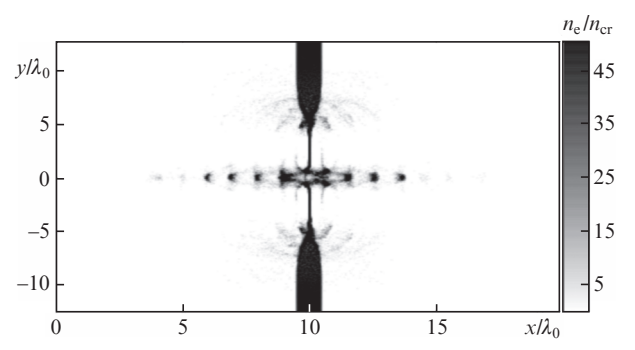

Figure 5. Cross section of the electron density in the xy plane with a fixed coordinate $z = 0\lambda_0$ at the interaction time $t \approx 2T_0$.

4. Conclusions

In this work, we have studied the interaction of a thin plasma target with two counterpropagating circularly polarised Laguerre–Gaussian laser pulses. In the first stage of the interaction, the incoming laser pulses compress the plasma target until it becomes transparent for the laser light. After that, plasma electrons are trapped in the nodes of the resulting electric field structure. However, some electrons are also concentrated in the zero-intensity region of the doughnut mode. In the further course of the interaction, electrons are emitted in the form of a train of electron packets. Adjacent packets are separated by the laser wavelength and each electron packet itself has a duration of roughly 830 as. In addition, it has been shown that these packets move at an ultrarelativistic velocity. The observed asymmetry between left-and right-moving electrons could be attributed to the interplay between the orbital and spin angular momentum of the circularly polarised Laguerre–Gaussian pulses.

More studies are necessary to consider the influence of laser parameters (e.g. pulse duration or transverse beam width) on the transverse and longitudinal spread of emitted electron packets, as well as on the beam quality. The configuration in question can be potentially used for many experimental situations which require the resolution of physical processes on very short timescales.

Acknowledgements. The authors acknowledge the financial support from the GSI Helmholtzzentrum für Schwerionenforschung in Darmstadt, Germany. One of the authors (C.B.) also thanks Camilla Willim for useful discussions about Laguerre–Gaussian laser modes.

References

1. Yanovsky V., Chvykov V., Kalinchenko G., Rousseau P., Planchon T., Matsuoka T., Maksimchuk A., Nees J., Cheriaux G., Mourou G., et al. *Opt. Express*, **16**, 2109 (2008).
2. *Extreme Light Infrastructure Project*, www.eli-laser.eu.
3. *Exawatt Center for Extreme Light Studies*, www.xcels.iapras.ru.
4. Di Piazza A., Müller C., Hatsagortsyan K., Keitel C. *Rev. Mod. Phys.*, **84**, 1177 (2012).
5. Ji L., Pukhov A., Kostyukov I.Y., Shen B., Akli K. *Phys. Rev. Lett.*, **112**, 145003 (2014).
6. Gonoskov A., Bashinov A., Gonoskov I., Harvey C., Ilderton A., Kim A., Marklund M., Mourou G., Sergeev A. *Phys. Rev. Lett.*, **113**, 014801 (2014).
7. Jirka M., Klimo O., Bulanov S., Esirkepov T.Z., Gelfer E., Bulanov S., Weber S., Korn G. *Phys. Rev. E*, **93**, 023207 (2016).
8. Baumann C., Pukhov A. *Phys. Rev. E*, **94**, 063204 (2016).
9. Vieira J., Trines R., Alves E., Fonseca R., Mendonça J., Bingham R., Norreys P., Silva L. *Phys. Rev. Lett.*, **117**, 265001 (2016).

10. Liu C., Shen B., Zhang X., Shi Y., Ji L., Wang W., Yi L., Zhang L., Xu T., Pei Z., Xu Z. *Phys. Plasmas*, **23**, 093120 (2016).
11. Naumova N., Sokolov I., Nees J., Maksimchuk A., Yanovsky V., Mourou G. *Phys. Rev. Lett.*, **93**, 195003 (2004).
12. Liseykina T., Pirner S., Bauer D. *Phys. Rev. Lett.*, **104**, 095002 (2010).
13. Pukhov A. *J. Plasma Phys.*, **61**, 425 (1999).
14. Goldsmith P.F. *Quasioptical Systems: Gaussian Beam Quasioptical Propagation and Applications* (New York: IEEE press, 1998) p. 28.
15. Elkina N., Fedotov A., Kostyukov I.Y., Legkov M., Narozhny N., Nerush E., Ruhl H. *Phys. Rev. Special Topics – Accelerators and Beams*, **14**, 054401 (2011).
16. Gonoskov A., Bastrakov S., Efimenko E., Ilderton A., Marklund M., Meyerov I., Muraviev A., Sergeev A., Surmin I., Wallin E. *Phys. Rev. E*, **92**, 023305 (2015).
17. Mironov A.A., Fedotov A.M., Narozhnyi N.B. *Quantum Electron.*, **46**, 305 (2016) [*Kvantovaya Elektron.*, **46**, 305 (2016)].
18. Allen L., Beijersbergen M.W., Spreeuw R.J.C., Woerdman J.P. *Phys. Rev. A*, **45**, 8185 (1992).